AFRL-ML-TY-TP-2007-4529

PREPRINT

ANALYTICAL ASSESSMENT OF THE BLAST RESISTANCE OF PRECAST, PRESTRESSED CONCRETE COMPONENTS

Nicholas Cramsey and Clay Natio
Lehigh University
1117 ATLSS Drive
Bethlehem, PA 18015

APRIL 2007

Interim report for 1 July 2006 – 30 November 2006

Submitted for publication in Fundamentals of Adsorption 9 special issue of Adsorption, Journal of the International Adsorption Society.

Air Force Research Laboratory
Materials and Manufacturing Directorate
Airbase Technologies Division
139 Barnes Drive, Suite 2
Tyndall AFB, FL 32403-5323

NOTICE AND SIGNATURE PAGE

Using Government drawings, specifications, or other data included in this document for any purpose other than Government procurement does not in any way obligate the U.S. Government. The fact that the Government formulated or supplied the drawings, specifications, or other data does not license the holder or any other person or corporation; or convey any rights or permission to manufacture, use, or sell any patented invention that may relate to them.

This report was cleared for public release by the Air Force Research Laboratory, Airbase Technologies Division Public Affairs Office and is available to the general public, including foreign nationals. Copies may be obtained from the Defense Technical Information Center (DTIC) (http://www.dtic.mil).

THIS REPORT HAS BEEN REVIEWED AND IS APPROVED FOR PUBLICATION IN ACCORDANCE WITH ASSIGNED DISTRIBUTION STATEMENT.

//signature//
PAUL SHEPPARD
Work Unit Manager

//signature//
JAMES A. HURLEY
Acting Chief, Force Protection Branch

//signature//
WENDELL D. BANKS
Chief, Airbase Technologies Division

This report is published in the interest of scientific and technical information exchange, and its publication does not constitute the Government's approval or disapproval of its ideas or findings.

REPORT DOCUMENTATION PAGE

Form Approved
OMB No. 0704-0188

PLEASE DO NOT RETURN YOUR FORM TO THE ABOVE ADDRESS.

1. REPORT DATE *(DD-MM-YYYY)*	2. REPORT TYPE	3. DATES COVERED *(From - To)*
30-APR-2007	Journal Article PREPRINT	01-JUL-2006 to 30-NOV-2006

4. TITLE AND SUBTITLE

Analytical Assessment of the Blast Resistance of Precast, Prestressed Concrete Components

5a. CONTRACT NUMBER

FA4819-07-D-0001

5b. GRANT NUMBER

5c. PROGRAM ELEMENT NUMBER

62102F

6. AUTHOR(S)

Cramsey, Nicholas; Natio, Clay

5d. PROJECT NUMBER

4915

5e. TASK NUMBER

F2

5f. WORK UNIT NUMBER

Q210FA72

7. PERFORMING ORGANIZATION NAME(S) AND ADDRESS(ES)

Lehigh University
117 ATLSS Drive
Bethlehem, PA 18015

8. PERFORMING ORGANIZATION REPORT NUMBER

9. SPONSORING/MONITORING AGENCY NAME(S) AND ADDRESS(ES)

Air Force Research Laboratory
Materials and Manufacturing Directorate
139 Barnes Drive, Suite 2
Tyndall AFB, FL 32403-5323

10. SPONSOR/MONITOR'S ACRONYM(S)

MLQF

11. SPONSOR/MONITOR'S REPORT NUMBER(S)

AFRL-ML-TY-TP-2007-4529

12. DISTRIBUTION/AVAILABILITY STATEMENT

Distribution Statement A: Approved for public release; distribution unlimited.

13. SUPPLEMENTARY NOTES

Submitted for publication in Fundamentals of Adsorption 9 special issue of Adsorption, Journal of the International Adsorption Society. Document contains color images.

14. ABSTRACT

Four blast tests were performed on 30-ft (9.1 m) tall precast, prestressed concrete wall panels. Two conventional sandwich panels and a control panel were examined and shown to perform adequately under the blast demands. An approximate dynamic analysis technique for finding the blast resistance of the wall panels was developed and validated using the experimental results. For the wall panels in this study, it was found that an undamped analytical model provided reasonable peak displacement approximations. Using the results from the undamped analytical model, conservative iso-damage curves were developed that characterize wall panel behavior subjected to varying levels of blast demands. It was found that accuracy of the iso-damage curve can be increased by accounting for the negative impulse regime. The analytical model is extended to assess the capacity of double tees subjected to a close-on explosion.

15. SUBJECT TERMS

blast loading, sandwich wall panels, experimental results, double tee, dynamic analysis, iso-damage curve

16. SECURITY CLASSIFICATION OF:			17. LIMITATION OF ABSTRACT	18. NUMBER OF PAGES	19a. NAME OF RESPONSIBLE PERSON
a. REPORT	b. ABSTRACT	c. THIS PAGE			Sheppard, Paul
U	U	U	UU	28	19b. TELEPHONE NUMBER *(Include area code)*

Reset

Standard Form 298 (Rev. 8/98)
Prescribed by ANSI Std. Z39.18

PCI Daniel P. Jenny Research Fellowship

Analytical Assessment of the Blast Resistance of Precast, Prestressed Concrete Components

Nicholas Cramsey[1] and Clay Naito[2]

SYNOPSIS

Four blast tests were performed on 30-ft (9.1-m) tall precast, prestressed concrete wall panels. Two conventional sandwich panels and a control panel were examined and shown to perform adequately under the blast demands. An approximate dynamic analysis technique for finding the blast resistance of the wall panels was developed and validated using the experimental results. For the wall panels in this study, it was found that an undamped analytical model provided reasonable peak displacement approximations. Using the results from the undamped analytical model, conservative iso-damage curves were developed that characterize wall panel behavior subjected to varying levels of blast demands It was found that accuracy of the iso-damage curve can be increased by accounting for the negative impulse regime. The analytical model is extended to assess the capacity of double tees subjected to a close-on explosion.

Keywords: Blast loading, sandwich wall panels, experimental results, double tee, dynamic analysis, iso-damage curve

Introduction

In today's climate, protection against blast has become a high priority for many clients. Blast retrofits and structural hardening, much like earthquake retrofits, can prove to be costly. For this reason, it is important to understand that inherent in any structural element is its capacity to absorb energy and resist explosions. Therefore, a general approach that allows a designer to realize the absorption capacity of a structural element may preclude the need for a blast specific retrofit. To illustrate this concept, the blast resistances of non-load bearing precast, prestressed concrete sandwich wall panels (WP) are examined. These components are used extensively in modern construction for cladding of building systems and often provide the primary level of protection from a blast event.

This paper investigates the behavior of precast, prestressed concrete WP's subjected to blast loads. Four blast tests were performed on four WP's. An analytical model was developed and validated with the

[1] Graduate Student Researcher, Lehigh University, 117 ATLSS Dr., Bethlehem, PA 18015, Email:ngc4@lehigh.edu

[2] Assistant Professor, Lehigh University, 117 ATLSS Dr., Bethlehem, PA 18015, Phone: (610)758-3081, Email:cjn3@lehigh.edu

measured blast demands and peak displacements. The analytical model is used to predict WP damage for varying levels of peak pressures and impulses. An extension of this method is proposed for assessing the blast resistance of horizontal diaphragm elements. The method is applicable for traditional precast diaphragm construction consisting of double tee (DT) or hollow core planks. An example analysis and design aids for a DT floor system with a localized blast is provided.

Background on Blast Demands

Blast demands on structures are generated by the detonation of a high explosive (HE) charge. After detonation, a chemical reaction occurs in which the solid (or liquid) HE changes into a gas in a very short period of time. The pressure loading generated is very complex and dependent on many factors including the type and size of explosive, the location of the explosive relative to the structure, and the objects between the HE and the structure.

The load effects generated by a blast can be divided into four components: over-pressure, impact of primary fragments, impact of secondary fragments, and reflected pressure [U.S. Army 1998]. Primary fragments are characterized as high velocity pieces of the explosive casing. They are typically ignored in structural design because of their size. Secondary fragments are objects that lie between the structure and the HE that are propelled as the blast wave expands from the detonation. While both of these demands can result in significant loss of life they are not commonly considered in the design of the structural system.

As the pressure loading expands outward from the detonation location a rise in the ambient pressure occurs. The magnitude of this pressure increase, or over-pressure, is dependent on both the amount of and radial distance (standoff) from the explosive. When the pressure wave comes in contact with an object in its path, an instantaneous rise in pressure above the over-pressure occurs. This pressure increase is termed reflected pressure. The reflected pressure demand is typically the controlling quantity for blast analysis and design of structural components. A reflected pressure demand is shown in Figure 1. The pressure arrives at time, t_a, after the detonation. The pressure instantaneously rises to P_{max}, the maximum reflected pressure, and decreases exponentially to a negative reflected pressure, P_{min}. The positive pressure occurs over a duration t_0. The energy of the blast demand can be characterized by the area under the pressure time curve. The area is divided into a positive impulse, I_p, and negative impulse, I_n.

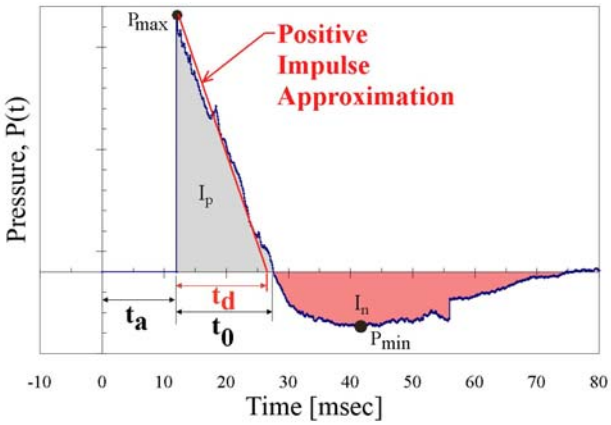

Figure 1: Reflected pressure demand

Reflected pressure versus time curves are typically approximated for dynamic analysis. For simplicity the negative impulse is ignored and the shape is estimated as a triangular pulse. The pulse is assumed to have the same I_p and P_{max} as the actual demand. A corresponding duration, t_d, can be determined (Figure 1). Typical blast demands have t_d values on the order of 10 to 20-msec. Due to the short time duration of explosive demands blast evaluation requires a structural dynamics approach.

Static versus Dynamic Evaluation

Design requires that the resistance of the structural component, R(y), be greater than the applied load demand, P (Equation (1)). For conventional demands such as wind or earthquakes, an equivalent static design procedure is used where the accelerations and velocities of the structure are assumed to be zero [ASCE 7-05]. Under a highly dynamic demand, $P(x,t)$, such as an explosion, the accelerations, $\ddot{y}$, and velocities, $\dot{y}$, of the structure become non-zero. As a consequence, the mass, M, and damping, C, of the structure can provide significant contribution to the resistance. Equation (2) presents the equation of equilibrium that must be satisfied under a dynamic condition. Clearly it is advantageous to have a structure with large mass and high damping under dynamic conditions; however, the same structure may be at a disadvantage in a static condition due to the high mass.

$$R(y) \geq P \qquad (1)$$

$$M * \ddot{y} + C * \dot{y} + R(y) = P(x,t) \qquad (2)$$

Approximate SDOF Method

To analyze a structural system under dynamic demands the equation of equilibrium must be evaluated incrementally. Dynamic analysis methods, such as the approximate SDOF (single degree of freedom) method, provide an efficient means for incremental evaluation. The approximate SDOF method is widely

accepted for blast analysis and used in practice. This method is presented in detail in Biggs [1964] and is outlined in Naito and Wheaton [2006]. A brief overview of the procedure is presented in the next several sections.

Equivalent Component

In a SDOF evaluation, the structure is evaluated at the component level. Each member of interest is uncoupled from the rest of the structure and analyzed individually. Appropriate boundary conditions are assumed, however, for simplicity simple support conditions are typically assumed. The use of simple supports results in the lowest stiffness which provides a conservative estimation of element deformation. The first floor WP and the second floor DT panel can be decoupled from the rest of the structure as shown in Figure 2.

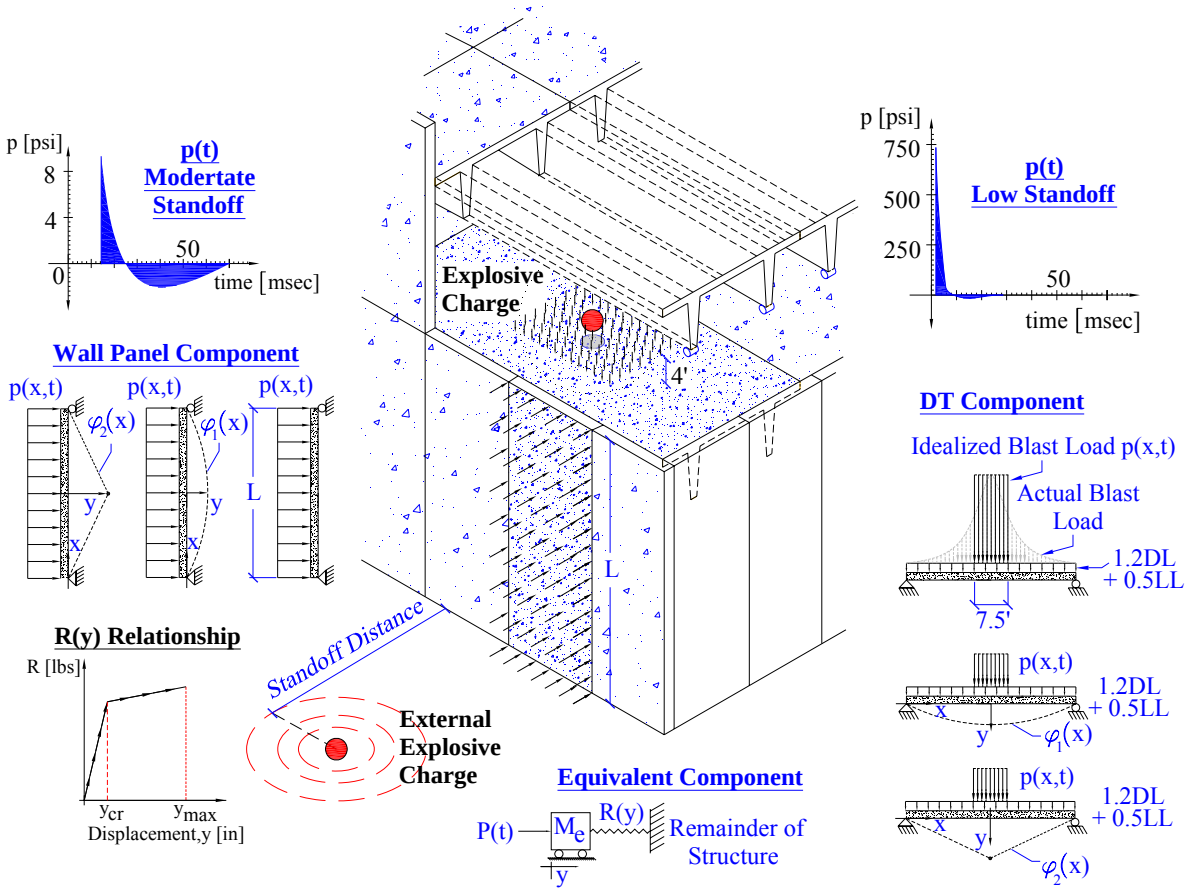

Figure 2: Wall Panel and Double Tee Idealization

Once the component is uncoupled from the structure, an approximate SDOF analysis is conducted. In the analysis, the real WP and DT components containing an infinite number of degrees of freedom (DOF) are reduced to an equivalent component characterized by one DOF (shown in Figure 2). Reduction to a one

DOF system is based on the assumption that the fundamental mode shape (or a close approximation of the fundamental mode) governs system behavior. This greatly reduces the computational effort required to perform the analysis. In this paper, mode shapes were derived based on the deflected shape resulting from static application of the blast pressure loads. Mode shapes Φ_1 and Φ_2 (shown in Figure 2) correspond to elastic and plastic response, respectively.

The one DOF equivalent component has an equivalent mass, M_e, total force, $P(t)$, and component resistance, $R(y)$, which are dependent on the assumed mode shape, boundary conditions and externally applied loading of the actual component. These aspects of the structural component are accounted for with a K_{LM} factor. The WP K_{LM} factors were formulated based on a uniform pressure load acting over the surface area and are presented in Table 1. The DT K_{LM} factors for different spans are also included. The equivalent undamped equation of dynamic equilibrium is shown as Equation (3).

Table 1: K_{LM} Factors (1-ft = 0.3048-m)

	$\Phi_1(x)$	$\Phi_2(x)$
WP	0.78	0.66
DT (40-ft span)	0.496	0.368
DT (45-ft span)	0.494	0.364
DT (50-ft span)	0.492	0.360
DT (55-ft span)	0.491	0.358

$$K_{LM} * M * \ddot{y} + R(y) = P(t) \quad (3)$$

Resistance of Structural Component, R(y)

The resistance of the component is characterized by a load-displacement (F - y) relationship computed according to standard procedures [Park and Paulay 1975]. The moment-curvature (M - ϕ) relationship of the cross-section is determined using a fiber analysis. For a given lateral pressure the moment distribution is determined. From the moment distribution and the moment-curvature relationship the curvature along the span can be determined. The displacement for the given curvature distribution is calculated using structural analysis principles. The lateral pressure is incremented to develop an entire, F-y relationship.

Structural Damping

In most blast analysis and design damping is ignored. Yet, in order to match the experimental results presented later in this paper, some form of damping must be included. A linear viscous, classical damping model was assumed. An approximate damping ratio for the fundamental mode shape was found by applying the log-decrement method to the measured response. The equivalent damped dynamic equation of equilibrium is shown as Equation (4). Damping varies with the damage in the structural component however the damping is considered constant for this application. For dynamic evaluation, Equations (3) or (4) can be solved incrementally using numerical integration.

$$K_{LM} * M * \ddot{y} + C * \dot{y} + R(y) = P(t) \quad (4)$$

Numerical Integration

Numerical integration was performed using Newmark's constant acceleration method for non-linear systems [Chopra 2001]. A time step of 0.1-msec was used for all models. The midspan displacement as a function of time is found for the actual system subjected to blast loading. The approximate SDOF method will be validated using experimental results in the next several sections.

Experimental Program

A series of four explosive detonations were conducted on four precast concrete wall panels at Tyndall Air Force Base (AFB) in Panama City, Florida. Three wall panel types were examined: a Control Panel (CP), Solid Zone Panel (SZP), and Carbon Fiber Reinforced Polymer Panel (CFRPP). The test structure, shown in Figure 3, supported two panels per detonation one in position A and the other in B. Table 2 displays the placement of each WP for each blast test.

Table 2: Testing Program

Test	Position A	Position B
1	Solid Zone Panel	Control Panel 1
2	Solid Zone Panel	Control Panel 1
3	CFRP Panel	Control Panel 2
4	CFRP Panel	Control Panel 2

The amount of explosive and standoff distance is restricted. The same amount of explosive was used in each test. The maximum standoff occurred in Test 1 (T1) and was subsequently decreased for the three remaining tests. Also, the SZP and CP tested in T1 were retested in T2 because no significant structural distress was apparent after T1. The CFRPP and CP tested in T3 were retested in T4.

Test Structure

A precast concrete testing structure was used for the blast evaluation (Figure 3). The structure was enclosed on all sides with access doors located on the rear of the structure. Simple support conditions are assumed for the WP. Schematics of the supports and front and side elevations are shown in Figure 3. The fixture was designed to have a 0.25-in. (0.64-cm) gap on either side of the panel however some binding was noted at the bottom 5-ft (1.52-m) of Position A. The test structure was fitted with 14 external pressure gauges and 6 displacement gauges. The location of the gauges can be seen in Figure 3. Displacement gauges were placed at ¼, ½, and ¾ height of each panel.

Panel Geometry

Three different WP's were tested: two conventional precast WP's and one control panel. WP elevations and cross sections are shown in Figure 4. The control panel had a solid cross-section and was conventionally reinforced (no prestressing was used). The cross section of the control panel was chosen to provide the same mass as the conventional panels.

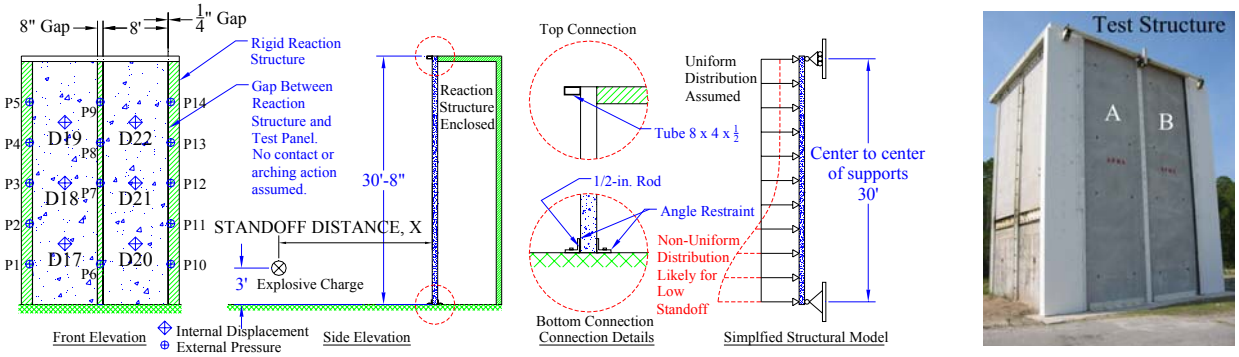

Figure 3: Test structure (Note: 1-ft = 0.3048-m; 1-n. = 2.54-cm)

The SZP and CFRPP were conventional insulated sandwich panels. The SZP contained solid zones of concrete connecting the exterior and interior wythes at 8 locations on the face of the panel and at each end. The solid zones at each end extended the full width of panel. The CFRPP contained only carbon fiber reinforcement between the wythes. The solid zones in the SZP and the CFRP in the CFRPP were present to provide a shear transfer mechanism between the exterior and interior wythe so that composite action could occur, no other mechanical connectors were present for shear transfer between the wythes. The SZP and CFRPP were assumed to provide 80% and 100% composite action, respectively.

In Figure 4d, the WP's are oriented such that the exterior panel face is on the bottom. Note that the CP contains #4 bar and welded wire reinforcement (WWR) and the sandwich panels contain prestressing strand and WWR. Sandwich WP's were pre-tensioned with 8 strands with an initial jacking force of 16.1-kips (71.6-kN) each. 25% prestressing losses were assumed.

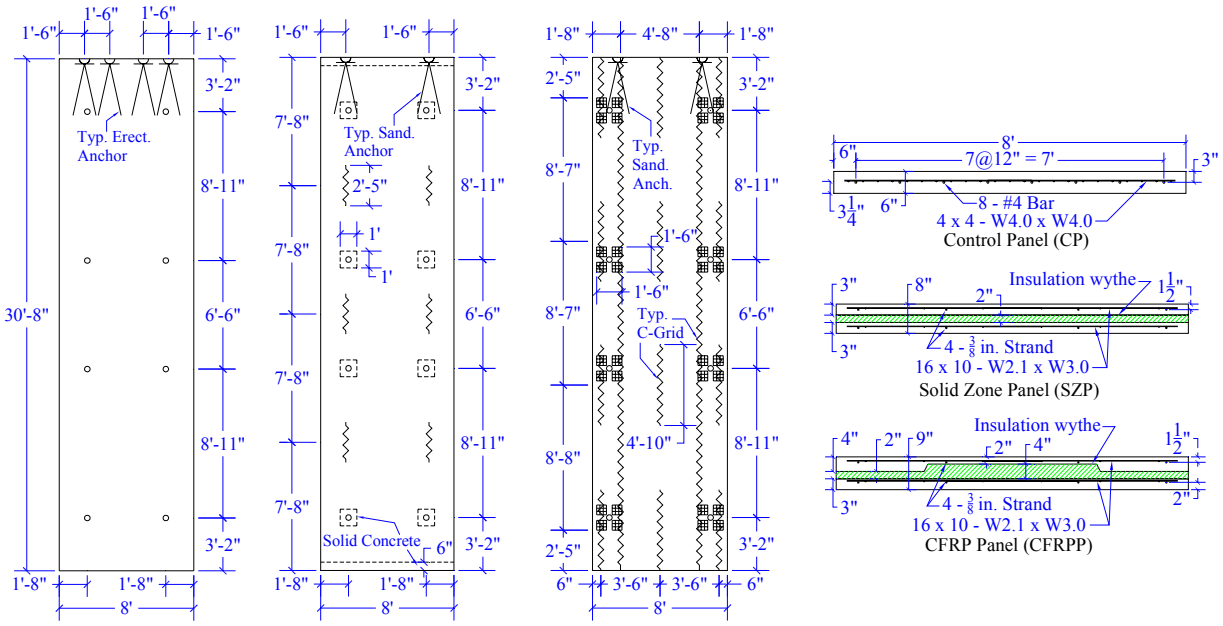

(a) Control Panel (b) Solid Zone Panel (c)CFRP Panel d) Wall Panel Cross Sections

Figure 4: Panel details (Note: 1-ft = 0.3048-m; 1-in = 2.54-cm)

Experimental Results

Results from the four blast tests are presented in Figure 5. Test 1 is presented in (a) and (b), T2 in (c) and (d), T3 in (e) and (f), and T4 in (g) and (h). Position A is shown on the left and B on the right. Each subplot within Figure 5 presents displacement versus time histories from each displacement gauge as identified in Figure 3. The reflected pressure time history of central pressure gauge, P7, is used. A secondary plot within each subplot shows a magnification of the response up to the first peak displacement.

The control panel exhibits consistently higher peak displacements and permanent deformation than the sandwich panels. The first peak displacement was the largest and was followed by rebound displacement of smaller magnitude. The sandwich panels exhibited much greater damping than the control panel. The high damping may be attributed to the prestressing or to partial binding of the panel against the test structure. Due to the questionable source of damping in the sandwich panels the damping of the control panel is used for the subsequent analysis.

In all cases the peak displacements occurred during or after the negative region of the impulse. This may be attributed to the high flexibility of the WP examined in this study. Shorter panel lengths (10 to 20-ft) (3.1 to 6.1-m) would significantly alter (increase) the stiffness and shorten the duration to the peak displacement. The plastic deformation occurring in T3 and T4 limited the first rebound displacement. Thus, it appears that when blast demands are increased, the first peak displacement would be the critical displacement.

Displacements are not uniform over the height of the wall. Differences are observed between the ¼ and ¾ point displacements (Figure 3). This variation may be due to marginal delay in arrival of the pressure wave over the height of the wall. From the reflected pressure gages the time of arrival varied from 1.5 and 2-msec over the wall. In addition, the variation could be attributed to the support movement observed at the base of the wall.

The peak pressure and positive impulse varied over the height and width of the wall with the highest value at the bottom center pressure gage. The variation was small with a coefficient of variation of less than 3% on the pressure and 10% on the positive impulse. Consequently a uniform pressure load assumption is assumed for the subsequent evaluations. The measured peak pressures ranged from 8 to 29-psi (55 to 200-kPa) with a positive duration from 16.4 to 15.1-msec and a positive impulse from 69.1-psi-msec (476.4-kPa-msec) to 144-psi-msec (992.8-kPa-msec) over the four tests. To reiterate the point that blast analysis requires dynamic evaluation, 8-psi is equivalent to 1152 lb/ft^2 (55-kPa). Designing the WP's for a static load of 1152-lb/ft^2 would be overly conservative.

Post test cracking diagrams are presented in Figure 6 for T2 and T3. Cracking is more extensive for the CP as compared to the sandwich panels. The crack size was largest at the mid-height and decreased toward the supports. A vertical crack was observed in the CFRPP post T3, this is indicative of two-way action at the bottom of the panel and may be due to binding between the panel and test structure. In all cases the panels performed well with distributed cracking and a permanent deformation of less than 3-in. (7.6-cm) over the 30-ft (9.1-m) span.

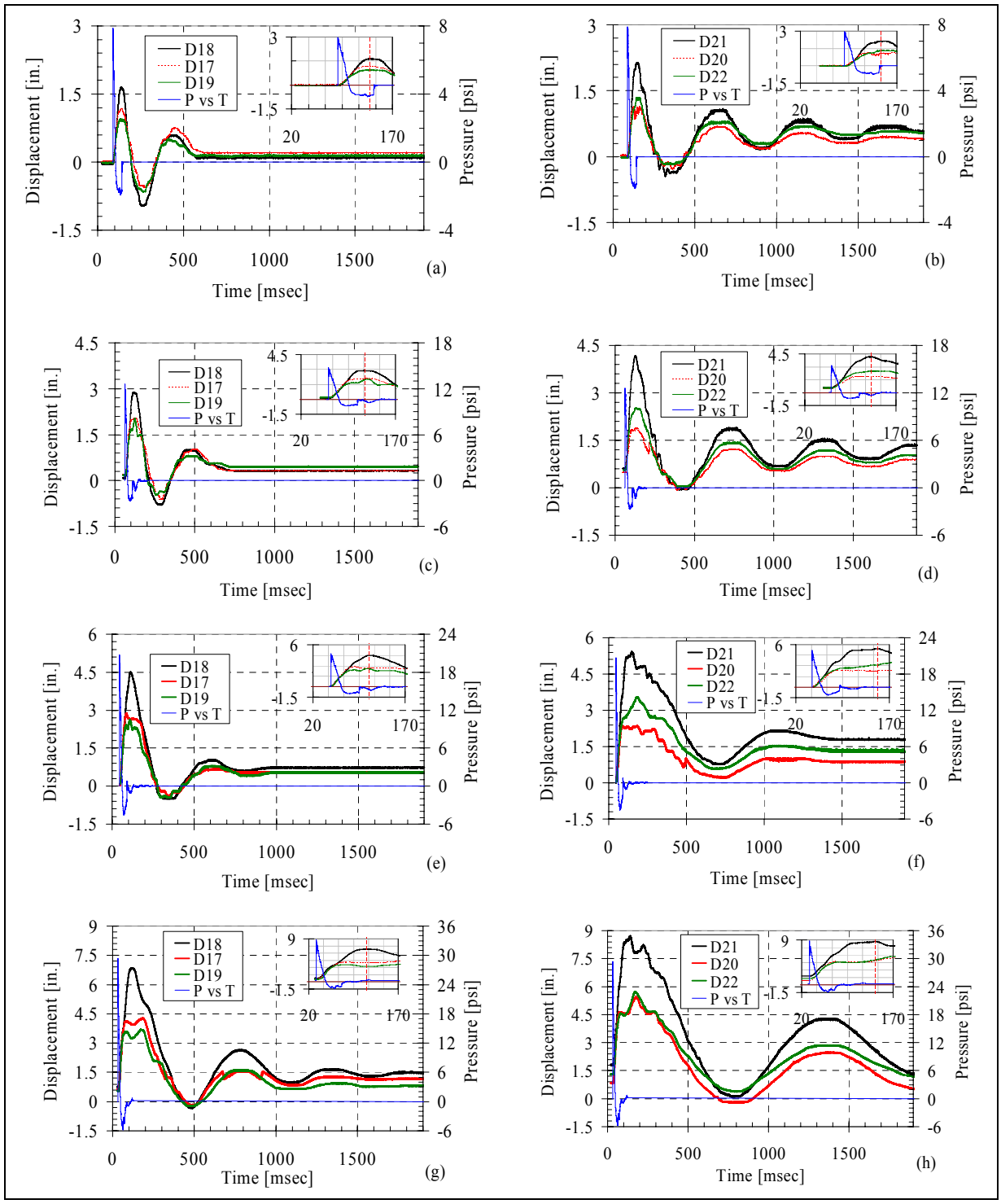

Figure 5: Displacement versus time response (Note: 1-in. = 2.54-cm)

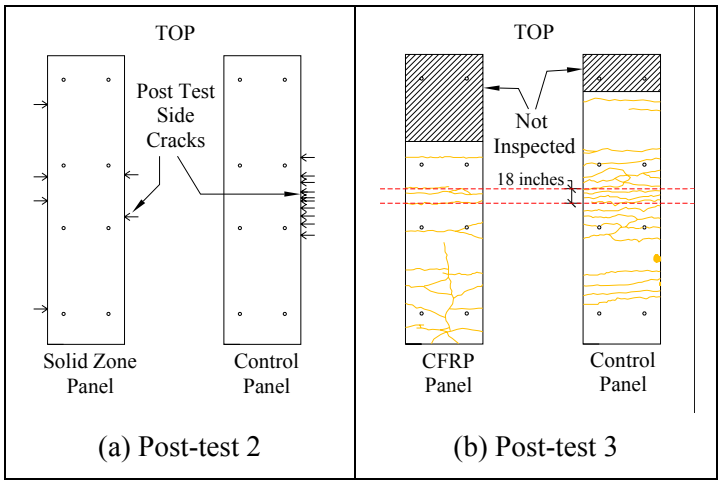

Figure 6: Post-test crack patterns (Note: 1-in. = 2.54-cm)

Predictive Modeling of Tested Wall Panels

The measured response is examined using an equivalent SDOF model based on the as-built conditions of the panels. The material properties and resulting moment-curvature and load-displacement responses are presented in this section.

Material Properties

The concrete 28-day compressive strength was 7.56-ksi (52.1-MPa), 8.90-ksi (61.4-MPa), and 8.60-ksi (59.3-MPa) for the CP, SZP and CFRPP, respectively. The linear piecewise approximate concrete stress-strain models are shown in Figure 7(b). It is assumed that the #4 bar met ASTM A706 specifications and the WWR met ASTM A185 specifications. The prestressing strands were 270-ksi (1862-MPa) low relaxation 3/8-in. (0.95-cm) diameter 7-wire strands. The mild steel reinforcement and WWR were modeled from recent mill certifications of similar material. Elastic moduli of the prestressing, mild steel, and WWR were assumed to be 29,000-ksi (200-GPa). The assumed in-situ static steel stress-strain models are shown in Figure 7(a).

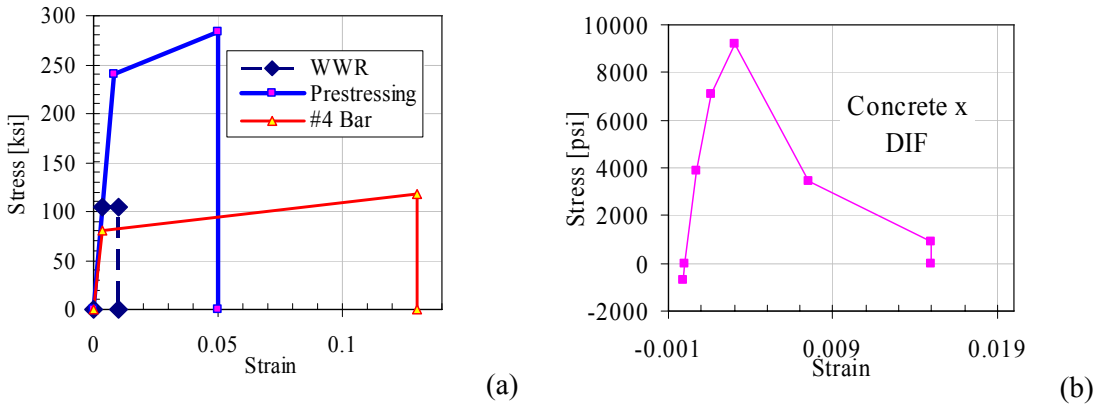

Figure 7. Material models (Note: 1-psi = 6.895-kPa)

Dynamic Increase Factors (DIF)

To account for material strength increases that occur under high strain rates the yield strength and strain and the ultimate strength of the concrete and steel were increased by a DIF. The strain rate was computed at the face of the wall and the location of the reinforcement from the measured displacement time history and the predicted moment curvature. The strain rates varied from 0.05 to 0.1/sec were estimated. A strain rate of 0.1/sec was used to compute the DIF values. The DIF are tabulated for different materials and strain rates in PSADS [U.S. Army 1998]. The DIF used are summarized in Table 3. DIF were not available for the ultimate strength of the WWR or for the prestressing strands. To be conservative a value of 1.0 is used.

Table 3: Dynamic increase factors (DIF)

Material	Yield	Ultimate
#4 Bar	1.15	1.05
WWR	1.05	1.00
Prestressing Strand	1.00	1.00
Concrete (Compression)	N.A.	1.20
Concrete (Tension/Shear)	N.A.	1.10

Moment-Curvature (M-Φ) Approximation

The *M-*ϕ analyses were performed using a fiber analysis technique. The CP was modeled as a solid concrete section composed of 300 fibers each 0.02-in. (0.05-cm) thick. The SZP and CFRPP were modeled as two solid concrete sections with fibers 0.02-in. (0.05-cm) thick. The layers of reinforcement were concentrated at their respective centroid locations (Figure 4(a)). The fibers were assigned material properties as previously presented in Figure 7.

For the sandwich WP's, fully composite (FC) and non-composite (NC) analyses were performed to provide a bound on the response. The insulation wythe (Figure 4d) was assumed to remain intact during the analyses and provide no structural resistance.

The results of the *M-*ϕ analysis for the tested panels are presented in Figure 8a. Due to cracking of the sandwich WP's a decrease in strength was observed. The resistance of the section increased as the tension reinforcement became effective (strands and WWR). This was followed by yielding of the tension reinforcement and fracture of the WWR. The sandwich WP's failed due to fracture of the prestressing strands in the tension wythe. The CP failed due to crushing of the concrete.

Approximate *M-*ϕ responses are developed from the non-linear estimates to simplify the SDOF analyses. The approximate curves characterize the behavior of the WP's to ultimate curvature as shown in Figure 8.

In estimating the ultimate response, a conservative equal energy approach was utilized. That is, the area under the predicted *M-ϕ* curve was found and used to develop an elastic perfectly plastic (EPP) ultimate curve. The elastic stiffness and the ultimate curvature were kept consistent. It is important to note that by maintaining an equal energy approach in determining the ultimate curve, energy absorption capacity is not fictitiously added to the system.

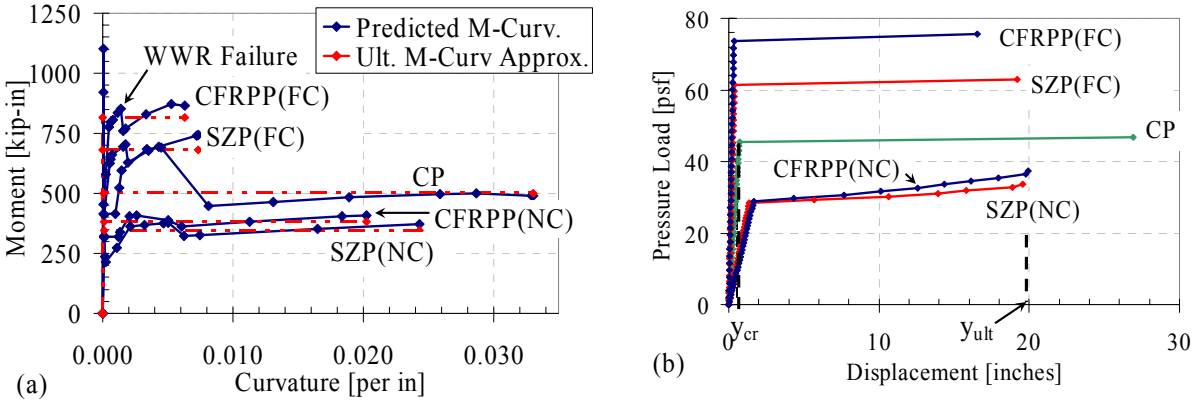

Figure 8: Estimated response (Note: 1 kip-in. = 0.13 N-m, 1-psf = 47.9-Pa, 1-in. = 2.54-cm)

Load-Displacement (F-y) Approximation

Using the approximate *M-ϕ* responses theoretical load - displacement relationships were determined and are presented in Figure 8b. Although the WP's were designed to have the same mass it is apparent from the *F-y* that the WP flexural capacities differ. The fully composite sandwich SZP and CFRPP can sustain approximately 33% and 66% more load than the CP. The extensive transverse cracking (Figure 6) of the CP can be attributed to the lower flexural capacity.

To determine the ultimate deformation a plastic hinge length (length over which maximum damage occurred) was estimated. A hinge length of 18-in. (45.7-cm) located at mid height was assumed. This corresponds to the region of concentrated transverse cracking observed in the tested panels as shown in Figure 6. The displaced shape at the ultimate deflection level is consistent with the shape function, Φ_2 shown in Figure 2. The estimated theoretical ultimate displacements (y_{ult}) are 19.2-in (48.8-cm) and 16.5-in (41.9-cm) for the SZP and CFRPP, respectively. The ultimate deflections correspond to support rotations of 6-degrees (0.105-radians) with approximately 2.7-in. (6.9-cm) of shortening and 5.1-degrees (0.089-radians) with approximately 1.6-in. (4.1-cm) of shortening for the SZP and CFRPP, respectively. The calculations do not account for P-δ effects which may reduce the ultimate displacement. This should be accounted for in load-bearing wall systems.

The CP ultimate deflection was limited based on the size of the supports. It was assumed that the WP could shorten 4-in. (10.2-cm) before it fell off its supports based on the WP boundary conditions (Figure

3). Using the ultimate deflection mode shape (Φ_2), this limited the CP ultimate displacement to 26.9-in. (68.3-cm). The CP ultimate deflection corresponds to a support rotation of 8.4-degrees (0.147-radians). It is important to note that this is a characteristic of the test setup only.

Once the maximum deformation, y_{max}, for the given demand is achieved the WP rebounds (Figure 5). Due to the damage that occurs in achieving y_{max} the rebound stiffness is not equal to the initial stiffness. To determine the appropriate stiffness to use for rebound and subsequent cycles the measured response is examined.

Rebound Stiffness Estimation

Figure 9(a) presents a schematic of a resistance versus displacement history for a typical WP subjected to blast load. During the initial positive displacement the WP follows the elastic and strain hardening stiffness, K1 and K2 previously determined from the load - displacement analysis (Figure 8b). After y_{max} is reached, the WP rebounds with a new stiffness K3 (softer than K1 due to the damage incurred) until a zero displacement is reached at midspan. At this displacement, it is assumed that the WP stiffness, K4, returns to the original stiffness, K1, as the uncracked (exterior) face, initially under compression experiences tension. Once the WP midspan rebounds back to zero displacement a final stiffness K5 is used. The K5 stiffness should be comparable to K3 if no additional damage is incurred during the rebound displacement. The stiffness intervals are defined in Figure 9(b) for clarity.

The initial rebound stiffness, K3, and the reloading stiffness, K5 are determined from the measured experimental results of the CP. Stiffness K3 was determined by minimizing the error between the measured displacement and the damped model at y_{reb}. Two methods were used to determine stiffness K5. In the first method, a fast fourier transform (FFT) was performed on the data within the K5 regime. The FFT provides the natural frequency, ω_n, inherent to the K5 regime from which the stiffness can be calculated using Equation (5). In the second method, one-half of the natural period of the WP, T_n, was estimated by calculating the time between a positive and subsequent negative peak displacement in the K5 regime (shown in Figure 9(b)). The stiffness can be calculated from the natural period estimation T_n. Stiffness calculated using the two methods correlated to within approximately 5% for T1.

$$\omega_n^2 = \frac{K5}{K_{LM} \bullet M} \qquad (5)$$

The resulting stiffness values for the CP model are summarized in Table 4. The resulting percentage decrease in stiffness from K1 is shown. Note that test 2 and 4 were conducted on damaged panels thus the initial stiffness for those two tests are assumed to equal the K5 stiffness from the preceding test. The

same stiffness degradation values are used for the sandwich WP's. These values are specific to the walls tested and may not be applicable to different systems or configurations.

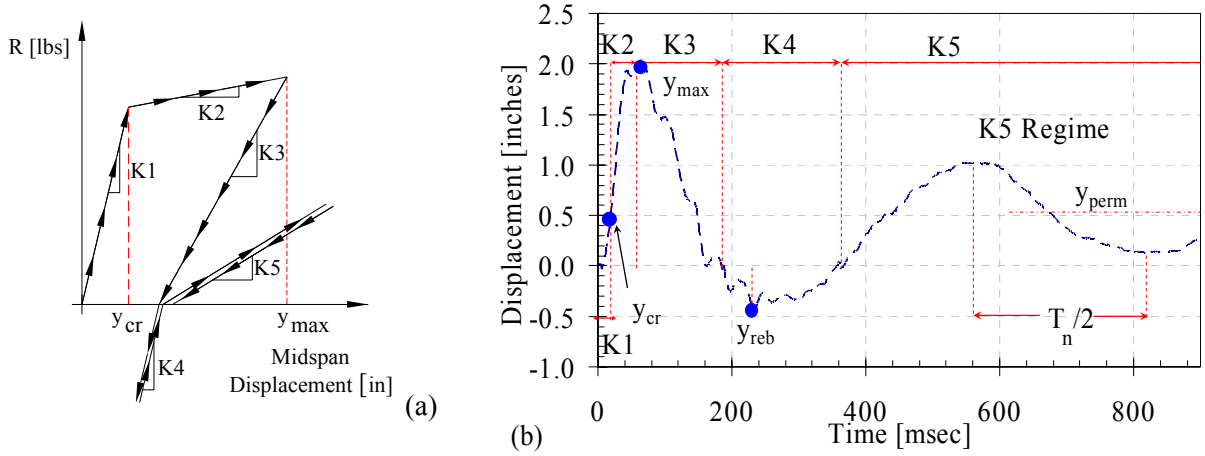

Figure 9: Rebound stiffness clarification (Note: 1-in. = 2.54-cm)

Table 4: Control panel stiffness rules (Note: 1-lb/in = 175.2-N/m)

	Test 1		Test 2		Test 3		Test 4	
Stiffness	Value [lbs/in]	% Initial	Value [lbs/in]	% Initial	Value [lbs/in]	% Initial	Value [lbs/in]	% Initial
K1	15564	100%	5060	33%	15528	100%	3882	25%
K2	356	2%	356	2%	416	3%	416	3%
K3	7159	46%	4046	26%	4813	31%	3571	23%
K4	15564	100%	15564	100%	15528	100%	n/a	n/a
K5	5060	33%	3950	25%	3882	25%	n/a	n/a

Critical Damping Ratio Estimation

Based on the measured responses a significant amount of damping was present in the tested panels. To model the displacement time history accurately a damping ratio is determined from the measured results. The log-decrement method was used to calculate the damping ratio whereby the peak displacements in free vibration, $y_{f,max\ 1}$ and $y_{f,max\ 2}$, were measured relative to the permanent deformation, y_{perm} (Figure 10). The peak displacements, permanent deformations, and damping ratios are summarized in Table 5 for T1 and 2. The lower critical damping ratio, ξ, of 10% is used in all analytical models to provide a conservative estimation of displacement.

Table 5: Critical damping ratio (ξ) (Note: 1-in. = 2.54-cm)

	Test 1	Test 2
$y_{f,\ max\ 1}$	1.02 in.	1.84 in.
$y_{f,\ max\ 2}$	0.74 in.	1.49 in.
y_{perm}	0.52 in.	1.11 in.

ξ	13%	10%

Experimental Validation for Control Panel

Using the approximate load-displacement response (Figure 8b), the stiffness rules (Table 4), and the applied reflected pressure time history from gauge P7, the approximate SDOF analysis was performed. The analyses were conducted for both undamped and with a 10% damping ratio. The predicted CP displacement - time histories are compared to the measured response for test 2 and 3 in Figure 10a and b, respectively. The undamped predictions are truncated after the first rebound displacement.

The predicted peak positive, y_{max}, peak rebound, y_{reb}, and permanent deformation, y_{perm}, are compared to the measured displacements in Table 6. The damped model consistently underestimates the peak displacement while the undamped model consistently over-estimates the peak displacement. To be conservative it is recommended that damping be ignored when maximum deformation is to be determined. The first rebound deformation is predicted more accurately with the damped model. The damped model also provides a conservative estimate of the permanent deformation.

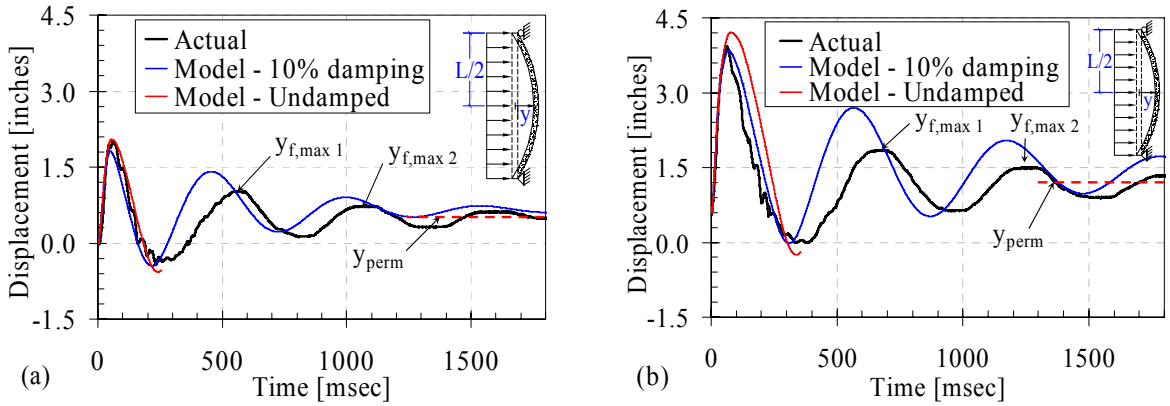

Figure 10: Analytical model validation (Note: 1-in. = 2.54-cm)

Table 6: Control Panel Analytical Model Displacement Comparison [in.]								
	Experimental			Model (10% damping)			Model (Undamped)	
Test	y_{max}	y_{reb}	y_{perm}	y_{max}	y_{reb}	y_{perm}	y_{max}	y_{reb}
1	2.02	-0.44	0.52	1.82 (-9.9%)	-0.45 (2.3%)	0.65 (25%)	2.05 (1.5%)	-0.58 (31.8%)
2	3.92	-0.02	1.11	3.85 (-1.8%)	-0.02 (0.0%)	1.25 (12.6%)	4.21 (7.4%)	-0.25 (1150%)
3	4.98	0.59	1.58	4.10 (-17.7%)	0.63 (-6.8%)	2.20 (39.2%)	5.19 (4.2%)	0.65 (-10.2%)
4	8.36	-0.11	2.25	7.92 (-5.3%)	-0.12 (9.1%)	n/a	9.11 (9.0%)	-0.45 (309%)

(Note: 1-in. = 2.54-cm; % Difference appears in ( ))

Experimental Validation for Sandwich Panels

The analytical model developed using the approximate SDOF method is extended to the sandwich wall panels. Unless otherwise stated, the same techniques used for the CP were used for the sandwich WP's. The results of the approximate undamped SDOF analyses for T2 and 3 are compared to the experimental response in Figure 11a and b, respectively. The peak and rebound displacements for all four tests are compared to the composite and non-composite model estimates in Table 7.

For all tests the assumption of full composite action provides a reasonable correlation with the measured peak displacement. Modeling the sandwich panels as non-composite significantly over-estimates the peak displacement. The rebound deformation was not accurately captured in either of the models. This may be attributed to a number of causes including but not limited to binding of the panel in the test fixture or variation in composite action over displacement history.

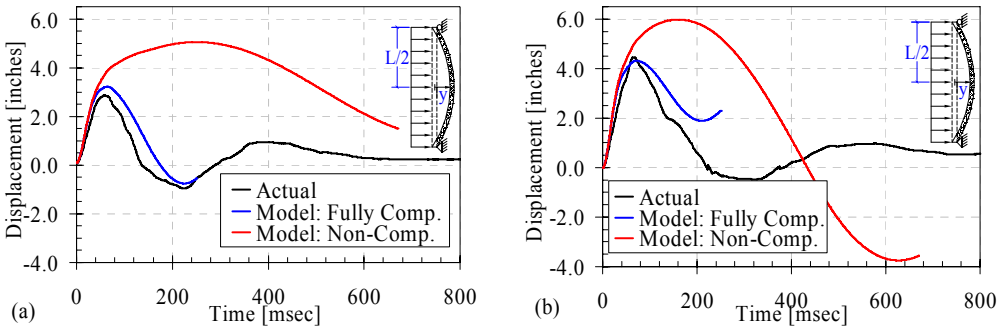

Figure 11: Sandwich panel analytical model (Note: 1-in. = 2.54-cm)

Table 7: Sandwich panel analytical model displacement comparison [in.]

	Actual		Model (Fully Composite)		Model (Non-Composite)	
Test	y_{max}	y_{reb}	y_{max}	y_{reb}	y_{max}	y_{reb}
1	1.52	-0.91	1.86 (22.4%)	-0.09 (90.1%)	2.19 (44.1%)	-2.89 (218%)
2	2.87	-0.95	3.22 (12.2%)	-0.75 (21.1%)	5.05 (76.0%)	1.12 (-218%)
3	4.46	-0.49	4.32 (3.1%)	1.89 (-486%)	5.97 (33.9%)	-3.75 (665%)
4	6.50	-0.31	6.11 (6.0%)	-0.75 (142%)	14.81 (128%)	0.32 (-203%)

(Note: 1-in. = 2.54-cm)

Reflected Pressure Approximation

As mentioned previously, reflected pressure versus time curves are typically approximated for dynamic analysis as a triangular pulse. To determine the adequacy of this approximation, the WP's were subjected to a triangular pulse equivalent to the positive phase of the measured reflected pressure versus time curves

from Figure 5. The resulting maximum displacements are compared in Table 8 to the displacements from the analytical model developed using the measured reflected pressure-time history (Table 6 and Table 7).

Table 8: Error in peak displacement [%]				
	Sandwich Panel		Control Panel	
Test	Actual P-t	Approx. P-t	Actual P-t	Approx. P-t
1	1.86 (22.4%)	5.35 (252%)	2.05 (1.5%)	8.04 (298%)
2	3.22 (12.2%)	10.03 (249%)	4.21 (7.4%)	16.54 (322%)
3	4.32 (3.1%)	>16.5 (>270%)	5.19 (4.2%)	>26.9 (>440%)
4	6.11 (6.0%)	>16.5 (>154%)	9.11 (9.0%)	>26.9 (>222%)

(Note: 1-in. = 2.54-cm, % Error w.r.t. experimental results)

It is apparent that the triangular pulse approximation is overly conservative for the WP's in this study. To accurately estimate the peak deformation of these panels the negative pressure phase must be included. This may not be the case for shorter panels. Recall from Figure 5 that all peak displacements occurred during or after the negative region of the impulse. Shorter panels will have increased stiffness which will cause the peak displacements to occur earlier. This will decrease the sensitivity of the peak displacement to the negative phase.

Generalized Blast Capacity Assessment

To determine the blast capacity of a structural component the equivalent SDOF modeling technique is used to develop iso-damage curves [Baker et al 1983]. Flexural iso-damage curves, FIDC, provide combinations of peak pressure, P_{max}, and a corresponding impulse, I_p, which cause the flexural capacity of the structural element to be achieved.

Flexural Iso-Damage Curves (FIDC)

To formulate a specific point on a FIDC using the triangular pulse approximation, a t_d value (Figure 12a) is assumed. P_{max} is then incrementally increased within the approximate SDOF method until the ultimate displacement of the wall was achieved. For the walls tested the following ultimate displacements were computed: 26.9-in (68.3-cm), 19.2-in (48.8-cm), and 16.5-in (41.9-cm) for CP, SZP, and CFRPP, respectively. The combination of maximum pressure and positive impulse that cause failure represent one point on the FIDC. The t_d was then increased and the procedure was repeated. A schematic of increasing triangular pulses and the corresponding displacement history for one value of t_d is shown in Figure 12a. The peak pressure and impulse causing failure is plotted on the flexural iso-damage curve in Figure 12b. The complete FIDC for the panels are presented in Figure 12b.

Given the amount of explosive and standoff distance the pressure and impulse demand can be computed using well established methods [U.S. Army 1998]. The peak pressure and impulse for a given amount of

explosive can be computed for multiple standoff distances and be incorporated into the FIDC as shown in Figure 12b. Pressure and impulse values to the left and below the FIDC would not cause failure; values on the other side would produce failure. For a given amount of explosive the panels will fail in a flexural mode at a standoff distance defined as X_{closer}. As the distance is increased to X and $X_{further}$ the demands decrease, this trend is captured in the explosive demand curve in Figure 12b. The actual standoff distances and explosive charge used are not shown due to security concerns.

It is important to note that the conservatism of the triangular pulse approximation is nested within the FIDC. To remove this conservatism, the negative pressure phase of the blast loading can be included in the formulation.

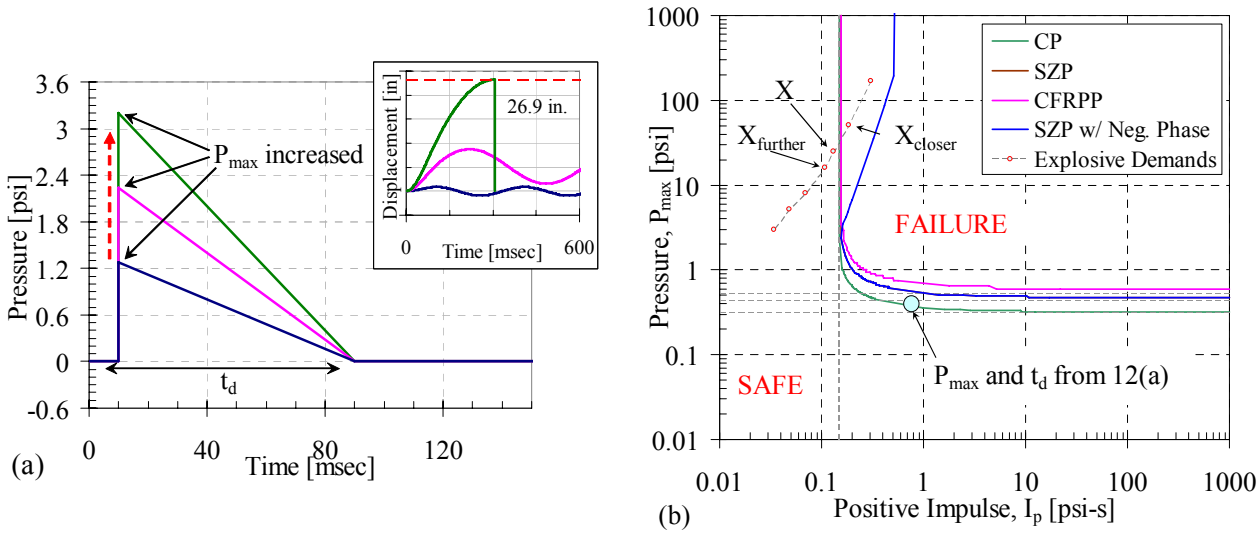

Figure 12: Flexural Iso-Damage Curves (Note: 1-psi = 6.9-kPa; 1-in. = 2.54-cm)

FIDC Including Negative Phase of Reflected Pressure

Developing FIDC including the negative reflected pressure phase of blast loads is a difficult task. No generalized pressure time response is available that characterizes P_{max}, P_{min}, I_p, t_o, and I_n for various standoffs and explosives. Consequently, the actual pressure – time history is used in place of the triangular pulse.

The reflected pressure versus time history corresponding to a small amount of explosive at a large standoff distance is generated using one of the tools available [Britt et. al. 2001]. The standoff distance is subsequently decreased until the reflected pressure - time history caused the WP ultimate displacement to be achieved. The amount of explosive was then increased and the procedure repeated. This procedure was conducted on the SZP. Since a realistic pressure –time history is used both a positive and negative impulse is applied. To characterize the response on a FIDC only the positive terms, P_{max} and I_p, are

included. The resulting FIDC (Figure 12b) indicates that the panel has a greater capacity than expected when compared to the triangular pulse approximation FIDC. The SZP which initially was expected to fail at a standoff distance, X_{closer}, is now capable of resisting the same explosive at an even closer standoff. Note that at very close standoff distances the uniform pressure load assumption may begin to breakdown. To account for the new pressure distribution, new K_{LM} factors may be required.

Shear Capacity

The structural component must also be evaluated for shear. This is accomplished by comparing the dynamic support reactions to the dynamic shear capacity. The dynamic reaction is determined from equilibrium of the dynamic system. Using the previously discussed mode shapes the shear demand can be found with respect to time. This procedure is summarized in Biggs [1964] and is presented in equations (6) and (7) for the elastic and plastic responses, respectively. The dynamic support reaction, *V(t),* is a function of the applied load, *P(t),* and resistance, *R(t),* at that time. The dynamic reactions were calculated using numerical integration and compared to the shear capacity. The shear capacity of the panels are found from the static shear strength of concrete ($2\sqrt{f_c'}$) with the DIF from Table 3 applied over the gross concrete area.

$$V(t) = 0.39 * R(t) + 0.11 * P(t) \qquad (6)$$

$$V(t) = 0.38 * R(t) + 0.12 * P(t) \qquad (7)$$

Figure 13 presents capacity and reaction demands for the third blast test. The support reactions for both panels are similar until approximately 55 msec. Since the resistance is low and demand is highest at the time of arrival the applied pressure load dominates the reaction force. The panel capacity is greater than the shear demand at all times.

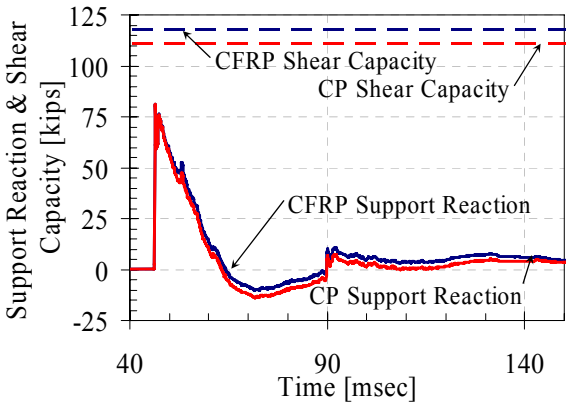

Figure 13: Test 3 shear capacity demand comparison (Note: 1-kip = 4.45-kN)

The techniques presented in the previous sections allow a designer to effectively analyze the blast capacity of a precast, prestressed concrete wall panel. The iso-damage curves including the negative pressure phase can be used as an effective blast evaluation tool.

Blast Capacity Assessment of Double Tees (DT)

The analysis techniques presented in the previous sections can be modified to simulate a close-on explosion (4-ft (1.2-m) standoff) on DT floor diaphragms. DT's of varying span lengths are examined and FIDC's are developed for each case.

Blast Demands

For a close-on explosion acting over the surface area of a DT, the blast loading is non-uniform. A simplified loading was developed to ease dynamic evaluation. A prototype structure was developed in BlastX [Britt et. al. 1998] similar to the structure in Figure 2. Seven different amounts of explosive, ranging from a briefcase to a vehicle sized explosive, were detonated at midspan of the DT, 4ft (1.2m) above the surface. For each explosive the peak pressures along the DT were found resulting in a non-uniform distribution. This was approximated with a uniform distributed load at midspan. For the uniform load the maximum pressure was kept constant and the width was chosen to produce the same total force as the non-uniform distribution. A uniform distributed load width of 7.5-ft (2.3-m) was found by averaging the results from each amount of explosive. A schematic of the original non-uniform and uniform approximation are shown in Figure 2.

Span lengths of 40-ft (12.2-m), 45-ft, 50-ft, and 55-ft were examined in this study. To reduce the actual system to an equivalent system, K_{LM}, factors were determined based on the approximate loading, DT length, and simply supported boundary conditions. The K_{LM} factors for the varying span lengths are summarized in Table 1.

Resistance

A 15-ft (4.6-m) wide DT cross-section is examined as shown in Figure 14. Sixteen ½-in. (1.3-cm) special low relaxation grade 270 (1862-MPa) prestressing strands were used with a constant eccentricity. Each strand has an initial jacking stress of 60% of ultimate, 18% prestressing losses were assumed. The DT is assumed to have the same steel material properties as the previously examined panels (Figure 7). The concrete is assumed to have a compressive strength of 6-ksi (41.4-MPa). The DT panels are designed to support self weight, D, and a live load, L, of 40-psf (1.9-kPa) in accordance with ASCE 7-05. The panels are designed to remain un-cracked under service loads.

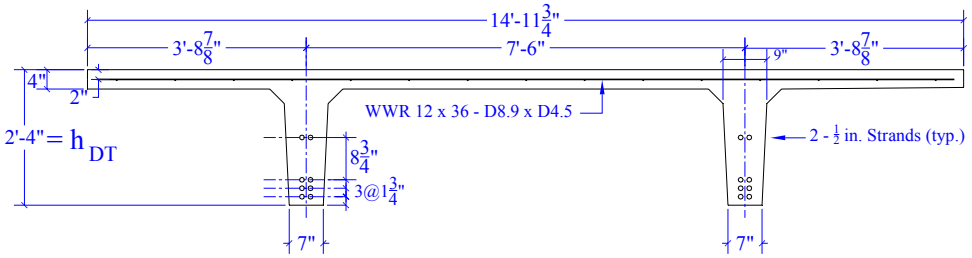

Figure 14: DT cross-section (Note: 1-in. = 2.54-cm)

Load-Displacement (F-Δ) Results

M-Φ analyses were performed and *F–y* results generated for each DT span length. A plastic hinge length of twice the depth of the DT was assumed for ultimate displacement calculations. The ultimate strength of the DT was controlled by fracture of the lowest layer of prestressing strand. It is assumed that the panels have adequate supports to prevent unseating. Prior to application of the blast load, a factored load of 1.2D + 0.5L, consistent with the Unified Facilities Criteria, was applied [U.S. DOD 2005]. The remaining DT capacity was available for blast resistance.

Analytical Model Application

The flexural iso-damage curves for the four DT span lengths are presented in Figure 15. The curves were formulated using the triangular pulse approximation as shown in Figure 12a. For the low standoff case examined the negative phase is negligible to that of the positive as shown in Figure 2. Using only the positive phase for this case should provide an accurate estimate of the panel capacity. These curves can be used to rapidly assess if the blast resistance is adequate.

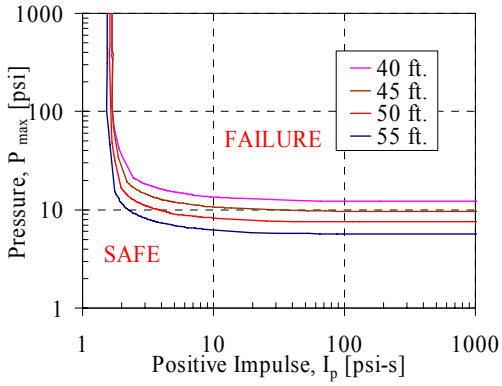

Figure 15: FIDC for double tee panels (Note: 1-psi = 6.9-kPa)

It is important to note that the extension of the model to DTs was purely analytical. Issues that may contribute to deviation from the presented results include but are not limited to the following: Brisance of concrete (local shattering of concrete) is possible for close-on explosions; contribution of adjacent DT panels to the flexural resistance; two-way flexural action could occur between the DT webs; finally,

higher order dynamic modes could contribute substantially to the behavior thus causing the analytical model to break down. Blast tests verifying the analytical model results would be beneficial.

Conclusions and Recommendations

Four precast wall panels were tested under four explosive demands. The pressure and displacement time histories of the walls were measured and are presented in detail. These results are used to validate approximate single degree of freedom (SDOF) models. Using these models flexural iso-damage curves can be developed for blast assessment of precast elements. The methods used to develop these curves and the accuracy of this method is presented. From the results and discussion presented the following conclusions can be made.

1. The precast, prestressed concrete wall panels subjected to peak pressures of 8 to 29-psi (55 to 200-kPa) and positive impulses of 69.1-psi-msec (476.4-kPa-msec) to 144-psi-msec (992.8-kPa-msec) performed adequately. Exhibiting distributed flexural cracking with a permanent deformation of less than 3-in. (7.5-cm) over the 30-ft (9.1-m) span.
2. The panels exhibited damping with a measured critical damping ratio of approximately 10%.
3. SDOF modeling methods provide a conservative approximation of deformation response for the precast concrete wall panels examined in this study.
4. To be conservative damping should be ignored when determining the maximum expected displacement.
5. If the displacement history is to be approximated, a damping ratio of 10% should be included for the wall panels in this study.
6. Modeling the sandwich wall panels as fully composite provided a reasonable approximation of peak wall displacement. Modeling the panels as non-composite provided overly conservative predictions.
7. Due to the flexibility of the wall panels examined in this study the peak displacement occurs during or after the negative pressure phase. Therefore the negative impulse must be included for accurate prediction of deformation. Discounting the negative phase provides an overly conservative estimation of expected deformation.
8. Accurate iso-damage assessment curves can be developed to account for the negative pressure phase by application of realistic pressure time histories.

9. Iso-damage curves can be developed for double tee floor diaphragm panels of various size, cross-section, and reinforcement. These models, however, are only theoretical and must be experimentally verified before used in practice.

Future Work

The analysis method presented is validated with experimental results from the Tyndall AFB precast wall panel tests. To fully validate the method for other applications additional blast testing of alternate wall panel types and floor diaphragm panels is imperative. In addition, the testing and evaluation method discussed assumes that the supports are capable of resisting the dynamic forces and resulting deformations imposed. Experimental validation of connection performance under blast demands should be conducted.

With further validation of double tee, hollow core and other precast panels the methods presented can be used to develop a database of FIDC's which would facilitate effective blast resistant design of precast concrete systems.

Acknowledgements

This analytical study was funded by the PCI Daniel P. Jenny Fellowship and Lehigh University. The experimental program was supported by the contributions of Portland Cement Association, Metromont, Inc., and the Precast/Prestressed Concrete Institute (PCI). Technical support was provided by Jeff Fisher of Tyndall AFB, Jason Krohn of PCI, Metromont Inc., members of the PCI Blast Committee, and High Concrete Structures. The authors would like to acknowledge these groups and individuals for their support. The findings and conclusions presented in this report are those of the authors, and do not necessarily reflect the views of the sponsors.

References

ACI Committee 318, "Building Code Requirements for Structural Concrete (ACI 318-05) and Commentary (ACI 318R-05)", American Concrete Institute, Farmington Hills, MI, 2005.

ASCE 7-05, "Minimum Design Loads for Buildings and Other Structures", American Society of Civil Engineers, Reston, VA, 2006.

Baker, W.E., Cox, P.A, Westine, P.S., Kulesz, J.J., Strehlow, R.A., "Explosion Hazards and Evaluation", Elsevier Scientific Publishing Company, New York, New York, 1983.

Biggs, J.M., *Introduction to Structural Dynamics*, McGraw-Hill Book Company, Inc., New York, 1964.

Britt, J.R., Ranta, D.E., and Joachim, C.E. (2001), "A User's Manual for the BlastX Code, Version 4.2." ERDC/GSL TR-01-2, U.S. Army Corp of Engineers, Engineering Research and Development Center, Geotechnical and Structures Laboratory, Vicksburg, MD.

Chopra, A.K., *Dynamics of Structures*, 2nd Edition, Prentice Hall, Upper Saddle River, New Jersey, 2001.

Naito, C.J, Wheaton, K.P, “Blast Assessment of Load Bearing Reinforced Concrete Shear Walls”, ASCE Practical Periodical on Structural Design and Construction, V. 11, No. 2, May, 2006, pp. 112-121.

Structures to Resist the Effects of Accidental Explosions, Department of the Army Technical Manual, TM5-1300, Department of the Navy Publication, NAVFAC P-397, Department of the Air Force Manual, AFM 88-22, Departments of the Army, the Navy, and the Air Force, June 1969.

U.S. Department of Defense (DOD), Unified Facilities Criteria (UFC), Design of Buildings to Resist Progressive Collapse, January 2005

U.S. Army Corp of Engineers. (1998), “Protective Structures Automated Design System (PSADS)”, Omaha, NE.